OPEN ACCESS

On the Degradation of Vanadium-Based Phosphate Framework Electrode Materials in Aqueous Environments

To cite this article: Davit Tediashvili *et al* 2023 *J. Electrochem. Soc.* **170** 120529

Journal of The Electrochemical Society, 2023 **170** 120529

On the Degradation of Vanadium-Based Phosphate Framework Electrode Materials in Aqueous Environments

Davit Tediashvili,[1,2] Jurgis Pilipavičius,[1,2] Jurga Juodkazytė,[1] and Linas Vilčiauskas[1,2,z]

[1]*Center for Physical Sciences and Technology (FTMC), LT-10257 Vilnius, Lithuania*
[2]*Institute of Chemistry, Vilnius University, LT-10257 Vilnius, Lithuania*

$Na_3V_2(PO_4)_3$ and $Na_3V_2(PO_4)_2F_3$ are among the most studied and applied positive electrode materials in non-aqueous sodium-ion batteries due to their relatively high capacities and redox potentials. However, the stability of these materials in aqueous environments is relatively low limiting their applications in aqueous batteries or deionization cells. In this study, we provide a comprehensive analysis of $Na_3V_2(PO_4)_3$ and $Na_3V_2(PO_4)_2F_3$ degradation in aqueous media using a number of techniques such as standard electrochemical methods, elemental analysis, powder X-ray diffractometry, and rotating ring-disc electrode. The latter allows for real time in situ/operando degradation analysis during electrochemical operation. The results show that $Na_3V_2(PO_4)_3$ suffers from chemical vanadium dissolution when immersed even in neutral pH electrolytes, whereas $Na_3V_2(PO_4)_2F_3$ is significantly more stable. The results obtained by the rotating ring-disc electrode technique explicitly show that at pH ~7 $Na_3V_2(PO_4)_3$ and $Na_3V_2(PO_4)_2F_3$ generate most of the soluble $V^{(V)}$ species during the electrochemical charging process. Whereas in acidic pH, there is also additional electrochemically-induced generation of soluble $V^{(IV)}$ species during the discharging process. The overall results suggest that fluoride ions significantly increase the structural stability of phosphate materials in aqueous environments. Potentially, a careful electrolyte design with controlled proton and water activity could enable the use of $Na_3V_2(PO_4)_2F_3$ in aqueous electrochemical devices.

 [DOI: 10.1149/1945-7111/ad13fa]

Manuscript submitted May 19, 2023; revised manuscript received October 31, 2023. Published December 26, 2023.

Efficient means of storing electrical energy remain one of the bottlenecks in utilizing intermittent solar and wind sources.[1,2] Alternative battery technologies based on abundant and easily recyclable materials are attracting a lot of attention.[3,4] Na-ion batteries are deemed to be one of such alternatives.[5–7] However, a significant research effort is still needed to develop high energy density, stable, and sustainable Na-ion battery materials. Due to their structural stability and structural diversity, phosphate framework materials are not only archetypical solid ion conductors but also are very suitable low-cost electrode materials for Na-ion batteries and other devices such as deionization cells.[8–10]

Vanadium-based NASICON-structured $Na_3V_2(PO_4)_3$ (NVP) and structurally related $Na_3V_2(PO_4)_2F_3$ (NVPF) with their relatively high specific charge capacity (117.6 mAh g^{-1} and 128.3 mAh g^{-1}, respectively) and high redox potential (3.4 V and 3.7/4.2 V vs Na^+/Na, respectively) are among the most studied and applied materials.[11,12] They also show high structural stability and reversibility for Na^+ extraction/insertion and are successfully used and commercialized cathode materials in non-aqueous Na-ion batteries.[13–18] However, the aqueous variation of Na-ion batteries is recently also attracting a lot of interest.[18–21] The use of aqueous electrolytes solves several problems simultaneously. They are inherently non-flammable, easy to produce, recycle and dispose, and show high conductivities.[18,20,21] Nevertheless, a number of issues primarily related to the stability of electrode/electrolyte materials in aqueous environments still need to be solved before their full potential could be realized.[18,20–23] In addition to the electrolytic decomposition of water, there is also transition metal dissolution (leaching) which is typically more pronounced in aqueous systems.[24–26] Vanadium dissolution into the electrolyte is widely assumed to be the main degradation process of most V-based electrode materials.[27,28]

A number of different experimental methods have been used to study the degradation of battery materials whether in situ/operando or post-mortem, such as various diffraction and spectroscopic techniques.[14,29–31] The electrochemical dissolution of electrode materials has been previously studied in situ/operando in specialized setups, e.g., different electroanalytical flow cells coupled with ICP-MS/OES.[30,32–35] However, electrochemical detection of dissolved metals is a simple and suitable method to study this process in battery electrode materials.[36] Rotating ring-disc electrode (RRDE) is a well-established technique which is readily available in most electrochemistry laboratories. Although it is typically used for studying the electrochemical processes under complete hydrodynamic control, recently it has also been successfully utilized to characterize e.g. dissolution/deposition processes.[37–40] For example, the dissolution products from the disc working electrode are forced by rotational convection towards the ring where they can be detected by applying an appropriate oxidative or reductive potential.[37,41] RRDE technique can provide useful insights into the degradation processes and has several advantages compared to more conventional methods used in battery materials research: (i) soluble degradation products are quickly swept away from the working electrode avoiding any undesirable side reactions, (ii) these products could be detected on the ring with insignificant time delay, (iii) the magnitude and time variation of recorded ring current could be used for quantitative determination of degradation extent with respect to the disc working electrode state of charge.

In this work, NVP and NVPF electrodes are studied in standard aqueous electrolyte solutions. The electrochemical performance is initially characterized by cyclic voltammetry (CV) in unbuffered (pH ~ 7) and citrate buffered (pH = 4) 1 M Na_2SO_4 (aq.). This is used to define general electrochemical conditions such as working potential windows. The extent of chemical and electrochemically-induced degradation of NVP and NVPF electrodes is assessed by double redox titration of spent electrolyte solutions. This technique allows for quantitative analysis of total vanadium content as well as its average oxidation state in studied solutions.[42–44] The analysis of electrode degradation is also supplemented by post mortem characterization using powder X-ray diffractometry (XRD), and scanning electron microscopy (SEM) coupled with energy dispersive X-ray spectroscopy (EDX). Finally, the RRDE technique is used for in situ/operando characterization of vanadium dissolution during the electrochemical operation of NVP and NVPF in unbuffered and citrate buffered (pH = 4) 1 M Na_2SO_4 (aq.) electrolyte solutions.

[z]E-mail: linas.vilciauskas@ftmc.lt

Experimental

Material synthesis.—$Na_3V_2(PO_4)_3$ samples were synthesized using the conventional solid-state method. In a typical synthesis, stoichiometric amounts of V_2O_5 (Thermo Fisher, 99.2%), Na_2CO_3 (Chempur, 99.8%), and $NH_4H_2PO_4$ (Honeywell, 99%) were mixed using wet (2-propanol) ball-milling (Retsch, PM 400) at 350 rpm for 2 h. The resulting mixture was dried at 70 °C and the powder was annealed in a tube furnace under a flowing forming gas (5% H_2 + 95% N_2) atmosphere for 4 h at 400 °C and 8 h at 800 °C with intermediate regrinding. The obtained powder was milled in a planetary ball-mill at 350 rpm for 2 h. In order to enhance its electronic conductivity, the powder was additionally coated with carbon by pyrolysis of citric acid (CA). For this purpose, NVP and CA were first dispersed in distilled water at 8:2 weight ratio, then dried at 70 °C, and annealed at 700 °C for 2 h in a flowing N_2 atmosphere.

$Na_3V_2(PO_4)_2F_3$ samples were prepared using aqueous sol-gel synthesis. In a typical synthesis, stoichiometric amounts of NaF (Chempur, 99%) and NH_4VO_3 (Reachem, 99.5%) were dissolved in deionized water. Next, stoichiometric amounts of $NH_4H_2PO_4$ (Honeywell, 99%) and citric acid (CA) (Lach-Ner, 100%) (molar ratio of V:CA = 1:0.8) were added into the same solution. The obtained solution was left on a hot plate overnight in order to evaporate water. The resulting powder was annealed at 300 °C for 4 h and then at 700 °C for 8 h in a flowing N_2 atmosphere with intermediate regrinding. The obtained NVPF powder had ∼5 wt% of carbon due to pyrolysis of CA as determined by thermogravimetric analysis (TGA). All obtained powders were additionally milled for 1 h at 350 rpm in order to achieve a uniform particle size distribution.

Structural and morphological characterization.—Powder X-ray diffraction patterns of the materials and electrodes were recorded on Bruker D2 Phaser X-ray diffractometer within the range $10° < 2\theta < 70°$ using Cu K_α radiation. The scanning speed and step width were 3° min^{-1} and 0.02°, respectively. The EDX analysis of the electrodes was performed on a table-top Scanning Electron Microscope (SEM) (Hitachi TM-6000) equipped with an EDX detector. Thermogravimetric analysis for the determination of carbon content in active material was carried out on PerkinElmer STA6000 analyzer in the temperature range of 30 to 700 °C at a heating rate of 10 °C min^{-1} in an air atmosphere (20 ml min^{-1}).

Electrode preparation.—The electrode slurry was prepared by dry mixing 70 wt% of active materials with 20 wt% of carbon black (CB) (TIMCAL Super-P, Imerys) in a planetary ball mill at 150 rpm for 1 h. After that, 10 wt% of polyvinylidene fluoride (PVDF) (Kynar HSV1800, Arkema) and N-methyl-2-pyrrolidone (NMP) (Sigma Aldrich, 99.5%) were added, and the slurry was additionally mixed in a ball mill for 2 h at 350 rpm. For the conventional cyclic voltammetry measurements, the slurry was cast as a film (ca. 300 μm) and dried in a vacuum oven (VO29, Memmert GmbH) for 3 h at 120 °C. The resulting electrode film was transferred onto 316L stainless steel mesh (#325) disks with an area of 1.33 cm^2 by pressing under a laboratory hydraulic press. The average active material loading was ∼2 mg cm^{-2} and ∼2.5 mg cm^{-2} in NVP and NVPF electrodes, respectively. For the RRDE experiments, the same slurry was drop-cast on a glassy carbon disc of RRDE tip and dried overnight. Prior to each RRDE measurement, the electrode was additionally dried in a vacuum oven for 1 h at room temperature resulting in active material loading of ∼4 mg cm^{-2}.

Electrochemical measurements.—Conventional cyclic voltammetry (CV) experiments were performed in a bottom-mount beaker-type three-electrode cell specifically designed for flat samples. Hg/Hg_2SO_4/sat. K_2SO_4(aq.) (MSE) (Redoxme AB) and graphite rod (Redoxme AB), or Ag/AgCl/sat. KCl (aq.) (Metrohm Autolab) and Pt sheet (Metrohm Autolab) were used as reference and counter electrodes in conventional CV and RRDE experiments, respectively. 1 M Na_2SO_4 (aq.) (Na_2SO_4 anhydrous, Alfa Aesar, 99%) was used as an electrolyte solution for electrochemical measurements unless specified otherwise. The electrolyte volume in the cell was 15 ml and 100 ml for CV and RRDE experiments, respectively. All electrochemical experiments were carried out at room temperature (ca. 20 °C) without any additional thermostatting.

All CV and RRDE measurements were carried out on a potentiostat-galvanostat (PGSTAT302N, Metrohm Autolab) equipped with a dual-mode bipotentiostat module capable to operate two separate working electrodes sharing the same reference and counter electrodes simultaneously. Galvanostatic charge/discharge specific currents were calculated based on the theoretical capacity of the respective materials. RRDE tip (Metrohm Autolab) was fitted with a 5 mm diameter glassy carbon disc and thin concentric platinum ring, separated by a 375 μm insulating gap. The RRDE rotation rate of 1200 rpm was used throughout this work.

Quantitative determination of vanadium content.—In order to evaluate the extent of chemical or electrochemical degradation of the electrodes, double redox titrimetry was carried out on the spent electrolytes after immersion and cycling. For this purpose, the collected electrolyte (ca. 12 ml) was transferred into a 25 ml measurement flask and filled with 4 M H_2SO_4 (aq.) (Lach-Ner). In order to ensure experiment repeatability, it was split into three identical samples (8.33 ml each) and titrated with 2.5 10^{-3} M $KMnO_4$ (aq.) (Chempur, 99.5%) until the color of the solution changed to purple, corresponding to full oxidation of all vanadium species to $V^{(V)}$. Subsequently, $V^{(V)}$ was reduced back to $V^{(IV)}$ by adding an excess of $(NH_4)_2Fe(SO_4)_2$ (Chempur, 99.5%). The remaining iron was oxidized to $Fe^{(III)}$ by adding $(NH_4)_2S_2O_8$ (Chempur, 98%) to avoid any undesired interference between $Fe^{(II)}$ and MnO_4^-. The final titration, corresponding to the oxidation of $V^{(IV)}$ into $V^{(V)}$ was performed with the same $KMnO_4$ (aq.) solution. This procedure provides information not only on the total vanadium concentration but also its average oxidation state in solution.[42–44]

In order to determine the amount of vanadium remaining in the cycled electrodes, they were transferred into 2 M HNO_3 (aq.) (Lach-Ner) solution and dissolved with the assistance of an ultrasonic bath. The remaining insoluble solid particles mainly containing carbon and PVDF binder were separated in a centrifuge. The solution was analyzed quantitively using Perkin Elmer Optima 7000DV inductively coupled plasma optical emission spectrometer (ICP-OES) to determine the vanadium elemental concentration. Calibration was performed by preparing appropriately diluted stock standard solutions (single-element ICP standards 1000 mg l^{-1}, Roth).

Results and Discussion

General electrochemical characterization.—The (electro)chemical degradation of NVP and NVPF electrodes was studied under different (electro)chemical conditions: (i) chemical dissolution due to immersion in an electrolyte, (ii) potentiodynamic cycling (CV), and (iii) galvanostatic cycling (GCD) in 1 M Na_2SO_4 (aq.) electrolyte solutions. Vanadium dissolution from the phosphate into the electrolyte is assumed to be the main degradation process in NVP and NVPF responsible for electrochemical activity and capacity loss. The amount of vanadium dissolved in the electrolyte under different conditions was quantitatively analyzed using double redox titrimetry. In addition, the amount of undissolved vanadium remaining in the electrode after a complete loss of electrochemical activity was analyzed by post mortem powder XRD and by ICP-OES.

In general, the electrochemical activity of NVP and NVPF materials is assumed to be related to the reversible $V^{(III)}/V^{(IV)}$ redox accompanied by (de)insertion of two sodium ions (out)/into the phosphate framework structure:

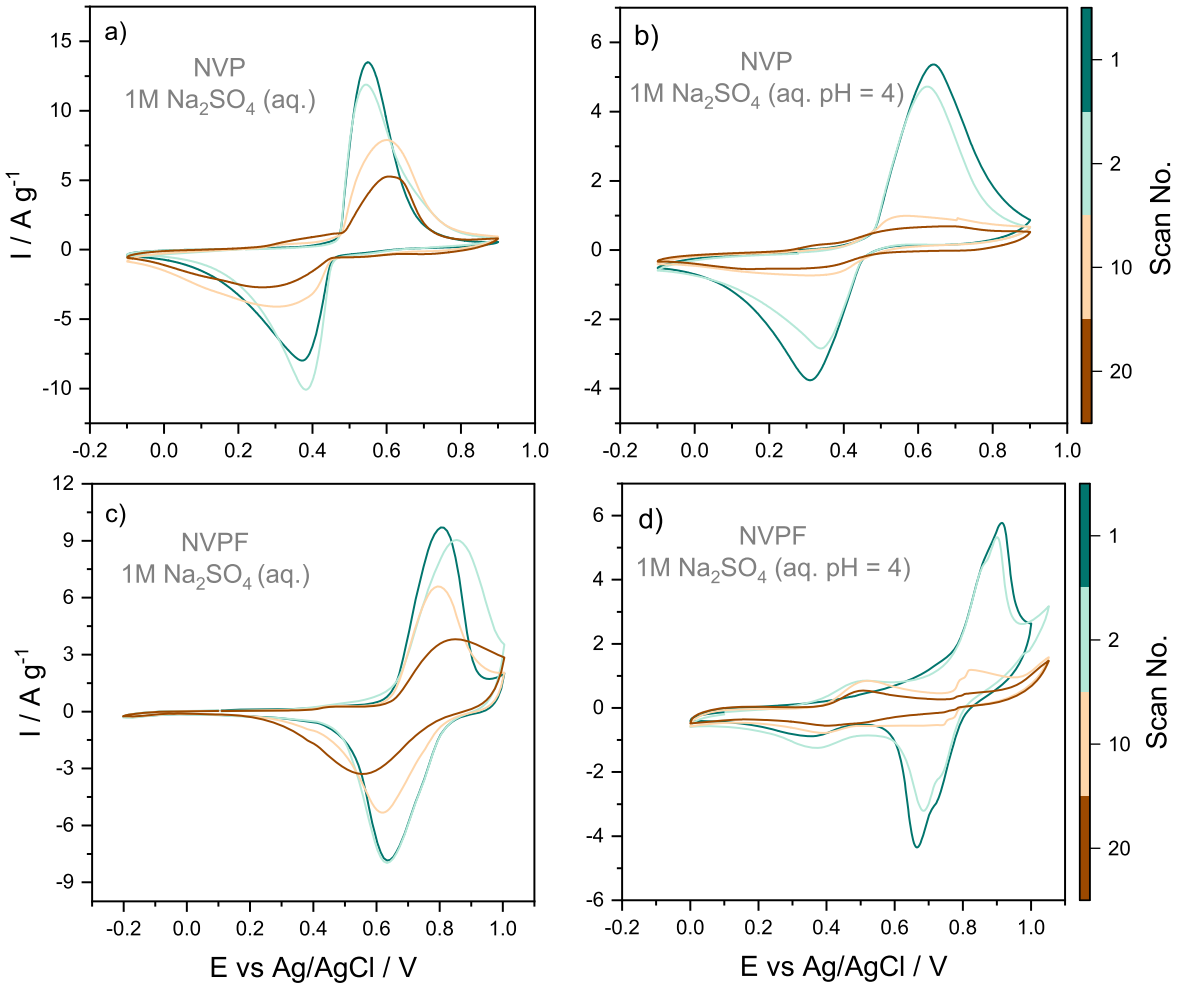

Figure 1. Cyclic voltammograms of $Na_3V_2(PO_4)_3$ (a, b) and $Na_3V_2(PO_4)_2F_3$ (c, d) electrodes corresponding to the 1st, 2nd, 10th and 20th scans recorded in unbuffered 1 M Na_2SO_4 (aq.) (a, c) and citrate-buffered 1 M Na_2SO_4 (aq. pH = 4) (b, d) electrolytes at potential scan rate of 5 mV s^{-1}.

$$Na_3V_2^{(III)}(PO_4)_3 \leftrightarrow NaV_2^{(IV)}(PO_4)_3 + 2Na^+ + 2e^- \quad [1]$$

$$Na_3V_2^{(III)}(PO_4)_2F_3 \leftrightarrow NaV_2^{(IV)}(PO_4)_2F_3 + 2Na^+ + 2e^- \quad [2]$$

Previous studies showed additional insertion of sodium into the crystal structure of NVP/NVPF leading to further reduction of $V^{(III)}$ to $V^{(II)}$.[45,46] However, this process is typically observed at low potentials (~1.7 V vs Na^+/Na) which are beyond the stability window of low concentration aqueous electrolytes, therefore it is excluded from further discussion.–

Initially, the materials were characterized by performing potentiodynamic cycling in flooded beaker-type bottom-mount cells filled with 1 M Na_2SO_4 (aq.). The cells were naturally aerated which resulted in pH ~6 in unbuffered 1 M Na_2SO_4 (aq.). An additional set of experiments was also performed in citrate (pH = 4) and borate (pH = 9) buffered electrolytes. The experiments at pH = 9 did not yield any noticeable difference from those in unbuffered solutions in terms of electrochemical activity or degradation. Therefore, they are omitted for brevity and clarity of presentation. The results obtained at 5 mV s^{-1} potential sweep rate are presented in Fig. 1. In the first CV scan, NVP shows a pair of reversible anodic/cathodic peaks at ~0.6/0.4 V vs Ag/AgCl, respectively (Fig. 1a). This activity starts to fade rapidly in subsequent cycles. Only very low capacity was recorded after 20 CV cycles and the change of electrolyte color to yellow which is characteristic to $V^{(V)}$ was observed. Based on vanadium Pourbaix diagram presented in Fig. 2, it is known that pH might have a strong effect on the oxidation state and stability of specific aqueous vanadium species.[47] Therefore, CVs were also recorded at pH 4 to assess the influence of the acidic environment on

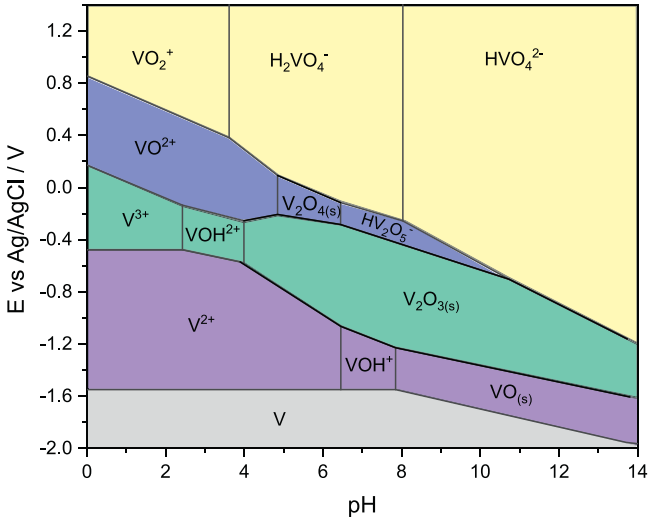

Figure 2. Pourbaix diagram for the vanadium—water system. Different colors represent different V oxidation states. Original data taken from Ref. 47.

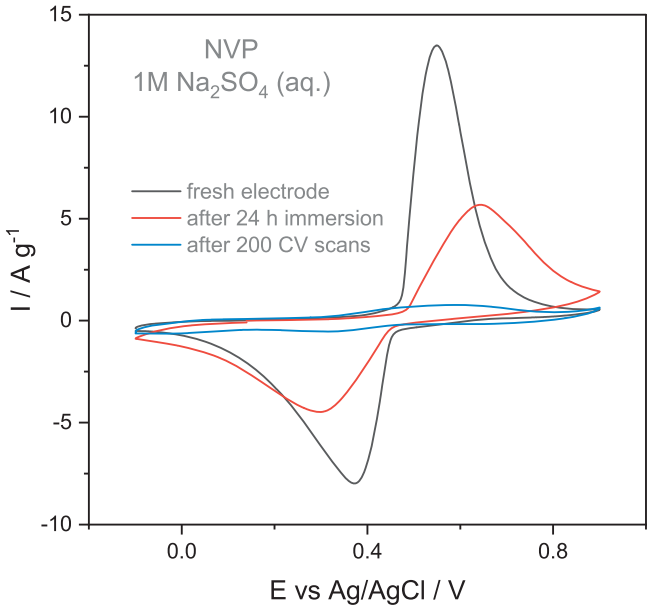

Figure 3. Comparison of NVP cyclic voltammograms in 1 M Na_2SO_4 (aq.) solution recorded for a fresh electrode (black), after 24 h electrode immersion (red), and after 200 CV cycles (blue) at 5 mV s^{-1}.

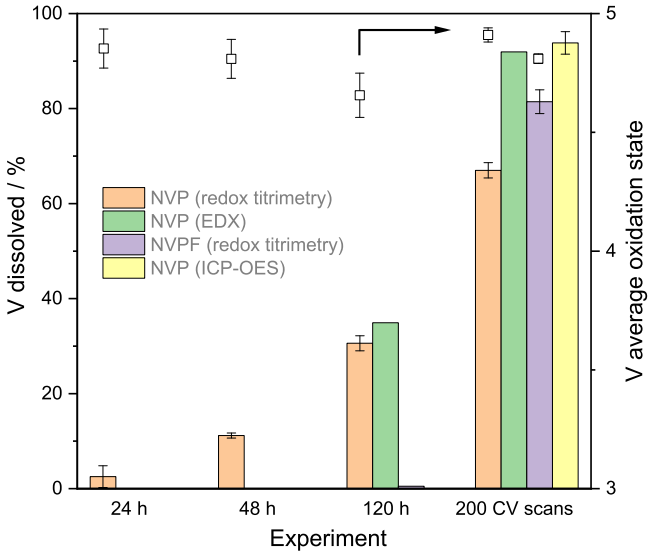

Figure 4. Assessment of chemical and electrochemical dissolution of NVP and NVPF in 1 M Na_2SO_4 (aq.). Fraction of dissolved vanadium as detected by redox titrimetry, EDX, or ICP-OES after either soaking NVP and NVPF electrodes for 24 h, 48 h and 120 h or performing 200 CV scans in 1 M Na_2SO_4 (aq.) electrolyte. Titrimetrically determined average oxidation state of V species in spent electrolytes (square symbols, right *y*-axis).

the stability of aqueous vanadium species (Fig. 1). Interestingly, the fade of NVP electrochemical activity is even faster in an acidic electrolyte suggesting that vanadium dissolution is accelerated under such conditions. A similar situation is observed in the case of NVPF as well. A pair of reversible anodic/cathodic peaks at ~0.85/0.65 V vs Ag/AgCl are observed in CV (Fig. 1c). The recorded currents start fading in subsequent potential scans similarly to NVP. This also indicates a significant capacity loss of NVPF when cycled in 1 M Na_2SO_4 (aq.). A similar behavior is also observed in the pH 4 experiment. NVPF capacity fades much faster in acidic than in near neutral conditions. It is worth mentioning that in the latter case some additional peaks at lower potentials start to show up in later cycles. It is difficult to identify their origin, but it could be related to the electrochemical activity of some dissolved vanadium species on the electrode surface. The electrolyte color changed to characteristic yellow during NVPF cycling as well. The capacity loss of NVP and NVPF under galvanostatic cycling conditions was quantitively very similar to that observed under potentiodynamic conditions. Therefore these results are omitted from further discussion for brevity and clarity.

Some previous studies on other NASICON structured materials such as $NaTi_2(PO_4)_3$ or $Na_3MnTi(PO_4)_3$ found that most of the capacity fade was not directly related to metal dissolution but rather to the loss of contact between active material particles. The main reasons being partial dissolution, amorphization, and formation of blocking interphasial layers on the particle surface.[37,48] The results presented in Fig. 3 show that the electrochemical response of NVP electrode as estimated by CV was reduced by more than 50% after it was immersed for 24 h in 1 M Na_2SO_4 (aq.). In order to understand the chemical and electrochemical details of NVP and NVPF capacity loss in aqueous electrolytes, vanadium dissolution process was quantitatively analyzed using a number of different techniques (Fig. 4). First of all, NVP electrodes were cycled for 200 CV cycles at 5 mV s^{-1} until virtually no electrochemical response attributable to vanadium redox was observed (Fig. 3). Then the electrolytes were collected and analyzed using double redox titrimetry. This method allows to not only determine the overall dissolved vanadium content but also its average oxidation state in solution. The results presented in Fig. 4 indicate that at least 66% of initial vanadium is dissolved from the electrode into the electrolyte during cycling. The average oxidation state of vanadium species found in the electrolyte is 4.9 ± 0.03 (Fig. 4), which supports the view that $V^{(V)}$ is the dominant species in aqueous medium. In addition, the amount of vanadium remaining in the electrode was determined post mortem by dissolving them in 2 M HNO_3 (aq.) and analyzing the obtained solution using ICP-OES. The results in Fig. 4 show that only 7% of initial vanadium was still present in the electrodes after 200 CV cycles. These results suggest that the majority of capacity loss in NVP is due to vanadium dissolution from the NASICON structure into aqueous electrolytes.

The extent of chemical versus electrochemically-induced vanadium dissolution in NVP and NVPF was quantitatively analyzed by simply immersing and soaking the electrodes in 1 M Na_2SO_4 (aq.) electrolyte solution for 24 h, 48 h, and 120 h. In the case of NVP, the characteristic yellow coloring indicating vanadium dissolution was observed already after 24 h. The results in Fig. 4 show that ca. 2.5%, 12%, and 30% of vanadium dissolved after 24 h, 48 h, and 120 h, respectively. This experiment suggests that chemical vanadium dissolution is an important contributor to the NVP capacity loss in low concentration aqueous electrolytes. The same experiment was also carried out for NVPF electrodes. Interestingly, virtually no vanadium dissolution from NVPF was detected even after 120 h (Fig. 4). This result suggests that contrary to NVP, chemical vanadium dissolution is such an important contributor to NVPF capacity loss in aqueous electrolytes.

In order to quantitively evaluate the extent of NASICON phase degradation, NVP electrodes were additionally studied *post mortem* using powder XRD and EDX. For this purpose, 20 wt% of HfO_2 was pre-mixed in electrode slurry during preparation and used as an inert internal standard. The powder XRD patterns (Fig. 5) and EDX elemental analysis (Fig. 4) were recorded for fresh electrodes, after 200 CV cycles, and immersion in 1 M Na_2SO_4 (aq.) for 120 h. The obtained results support our previous findings on significant degradation of NVP phase in aqueous electrolytes even without electrochemical cycling. A clear reduction of characteristic NVP XRD peaks is seen after electrode spends 120 h in electrolyte (Fig. 5a) and a drop in Hf:V ratio from 2.52 to 1.67 in EDX elemental analysis (Fig. 4). Furthermore, NVP phase is practically undetectable after 200 CV cycles as there are no visible NASICON peaks in XRD pattern (Fig. 5a) and only a negligible amount of vanadium could be detected by EDX (Fig. 4). A completely different situation is observed in the case of NVPF. Virtually no changes of characteristic

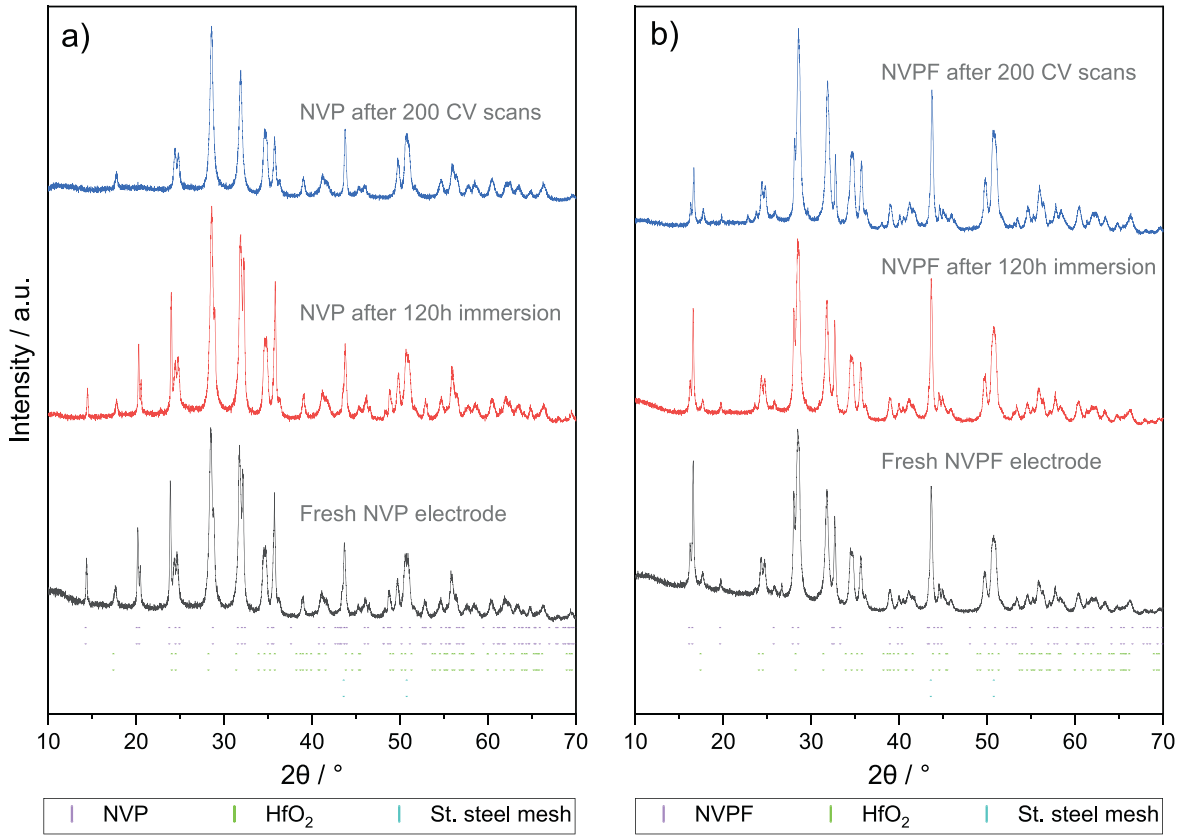

Figure 5. XRD patterns of (a) NVP and (b) NVPF electrodes containing 20 wt% of HfO_2 inert internal standard: fresh electrode (bottom-black), after 120 h soaking in 1 M Na_2SO_4 (aq.) (middle-red), and after 200 CV cycles at 5 mV s^{-1} in 1 M Na_2SO_4 (aq.) (blue-top). Most of the unmarked reflections correspond to the stainless steel mesh current collector.

NVPF XRD peaks are detected after electrode spends 120 h in electrolyte (Fig. 5b). Moreover, most of the characteristic peaks are only reduced but still easily visible after 200 CV cycles (Fig. 5b).

RRDE experiments.—Once the operating potential windows of NVP and NVPF electrodes are known, it is necessary to select the appropriate ring potential for analyzing the dissolved vanadium species in RRDE experiments. First, a set of CVs were recorded by sweeping the potential on the Pt ring electrode in: (i) fresh unbuffered, (ii) citrate buffered (pH = 4), and (iii) collected V-containing unbuffered 1 M Na_2SO_4 (aq.) electrolytes. The results presented in Fig. 6 suggest that in unbuffered electrolyte there is little background interference between −0.7 V and 1.2 V vs Ag/AgCl due to hydrogen and oxygen evolution, respectively. Once the pH is lowered to 4, the onset potential of hydrogen evolution shifts up to −0.4 V vs Ag/AgCl. This reduces the operating electrochemical window at pH 4. In the case of collected V-containing electrolyte, there is a significant electrochemical activity in the entire potential window from −0.7 V up to 1.1 V vs Ag/AgCl. This suggests that there could be a number of different vanadium species undergoing redox reactions in such a system. Throughout this work, $V^{(V)}$ is assumed to be the dominating species in solution according to the Pourbaix diagram (Fig. 2). $V^{(V)}$ could be generated intrinsically in the active material in the charge state by disproportionation:[49]

$$NaV^{(IV)}V^{(IV)}(PO_4)_3 \leftrightarrow NaV^{(III)}V^{(V)}(PO_4)_3 \quad [3]$$

$$NaV^{(IV)}V^{(IV)}(PO_4)_2F_3 \leftrightarrow NaV^{(III)}V^{(V)}(PO_4)_2F_3 \quad [4]$$

$V^{(V)}$ species could also be generated extrinsically by oxidation of $V^{(IV)}$ or $V^{(III)}$ species in aqueous environments.

In the case of a negatively polarized ring in RRDE experiment, the following reduction reaction to $V^{(III)}$ might be expected

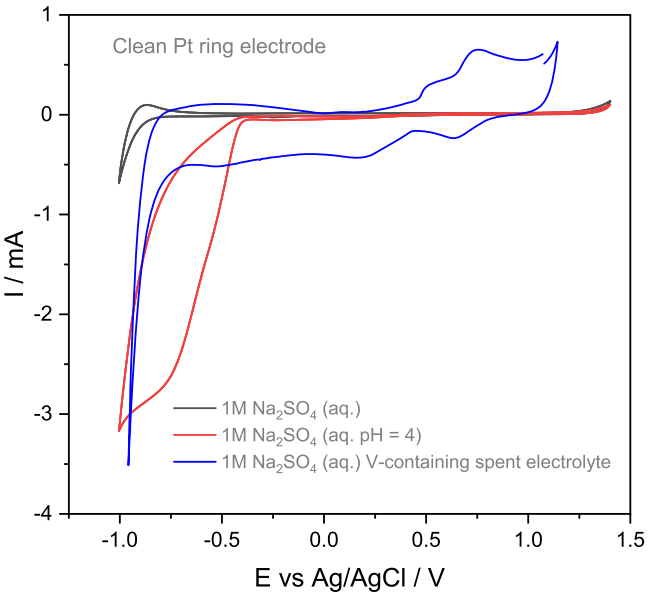

Figure 6. Cyclic voltammograms of clean Pt ring electrode in fresh unbuffered (black), citrate buffered (pH = 4) (red) and V-containing spent 1 M Na_2SO_4 (aq.) (blue) electrolytes recorded at 5 mV s^{-1}.

according to Fig. 2:

$$H_2VO_4^- + 2e^- + 5H^+ \rightarrow VOH^{2+} + 3H_2O \quad [5]$$

As suggested by our double redox titration results if some $V^{(IV)}$ is also present in the electrolyte, another reduction reaction might take

place on a ring:

$$VO^{2+} + e^- + H^+ \rightarrow VOH^{2+} \quad [6]$$

In the case of a positively polarized ring, it is either $V^{(IV)}$ species which can be oxidized to $V^{(V)}$:

$$VO^{2+} + 3H_2O \rightarrow H_2VO_4^- + 4H^+ + e^- \quad [7]$$

or $V^{(III)}$ species which might be oxidized to $V^{(V)}$ in a two-electron process:

$$VOH^{2+} + 3H_2O \rightarrow H_2VO_4^- + 5H^+ + 2e^- \quad [8]$$

A number of independent RRDE experiments were done potentiodynamically and galvanostatically in unbuffered and pH 4 buffered 1 M Na_2SO_4 (aq.) electrolytes. Two different Pt ring electrode polarization modes were selected to study possible reduction and oxidation processes of dissolved vanadium species. The ring was kept at −0.7 V or at −0.4 V in pH = 4 vs Ag/AgCl for reductive and at 1.2 V vs Ag/AgCl for oxidative processes. In all experiments, the ring current was stabilized for 0.5 h before disc polarization. The results presented in Fig. 7 show disc voltammograms and ring chronoamperograms. The CVs look similar to the ones obtained in a conventional cell (Fig. 1). The NVP degradation seems to be faster in the RRDE experiments. This could be attributed to (i) the much higher porosity of drop-casted electrode leading to higher electrochemically active surface area and electrolyte access, and (ii) faster removal of dissolved vanadium species due to forced convection which shifts the equilibrium and accelerates dissolution.

In the case of negative ring polarization, the ring current starts to increase markedly at the onset of the first anodic CV wave of the NVP disc (Fig. 7a). The ring current increases approximately until the disc anodic peak potential (0.6 V vs Ag/AgCl) is reached and starts decreasing afterward. Another small increase is also observed close to the disc anodic end potential (1 V vs Ag/AgCl), which is probably due to increasingly oxidative conditions. During the entire first disc cathodic scan, the ring current systematically decreases reaching negligible values at the cathodic end potential. This unambiguously indicates that $V^{(V)}$ species are generated from NVP during the entire charging process and not only at very high potentials. However, there is virtually no electrochemically-induced generation of $V^{(V)}$ during discharging. An identical set of experiments was also performed with a positively polarized ring in order to detect the presence of $V^{(IV)}$ and $V^{(III)}$ species. The results in Fig. 7a show the positive ring current values to be almost two orders of magnitude lower than the negative ones. This suggests that although there might be some lower oxidation state vanadium species present in electrolyte, their concentration is almost negligible with respect to $V^{(V)}$ which is generated during the charging of NVP.

In the case of pH 4 buffered electrolytes, similar disc CVs and negative ring current trends are observed as in the unbuffered case (Fig. 7b). Only the magnitude of disk currents decreases by about 50%. This is similar to conventional CV experiments (Fig. 1) and could be due to faster degradation in an acidic environment which reduces overall NVP electrochemical activity. It is further supported by the fact that the initial background current on the negatively polarized ring at pH 4 is about 5 times higher than that in an unbuffered electrolyte. Moreover, the negative ring current starts to increase before the onset of the disc anodic peak at 0.5 V vs Ag/AgCl (Fig. 7b) and there is a similar negative ring current increase during the reverse disc cathodic scan. All this suggests the presence of more chemically dissolved V species at pH 4. Another important observation is that there is also a peak of a positively polarized ring current (∼3 μA) on the first anodic disc scan at ∼0.4 V vs Ag/AgCl (Fig. 7b). This suggests that some of the V species could be also oxidized on the Pt ring electrode. The only species that can be both reduced and oxidized depending on the ring electrode polarization are $V^{(IV)}$. The results suggest that the chemical dissolution of NVP at

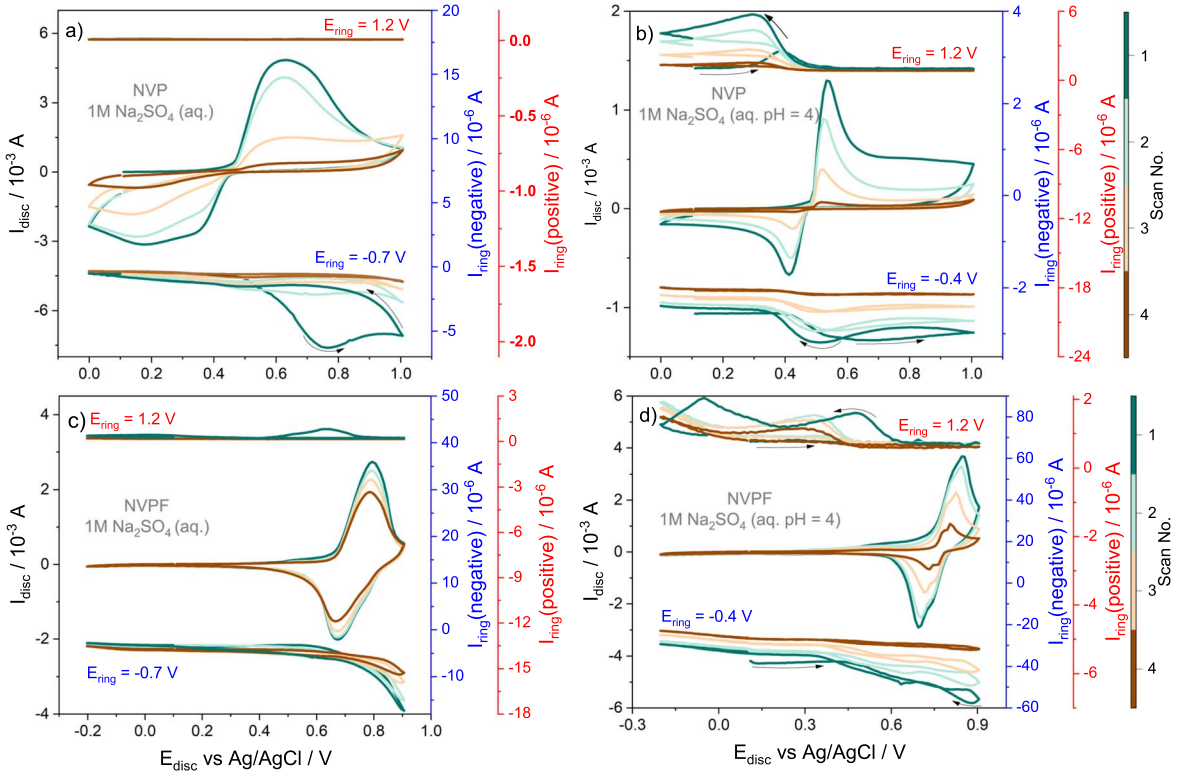

Figure 7. Cyclic voltammograms of RRDE disc electrode together with chronoamperograms of Pt ring electrode (right *y*-axes) corresponding to: (a) NVP in unbuffered 1 M Na_2SO_4 (aq.); (b) NVP in buffered 1 M Na_2SO_4 (aq. pH = 4), (c) NVPF in unbuffered 1 M Na_2SO_4 (aq.); (d) NVPF in buffered 1 M Na_2SO_4 (aq. pH = 4). Negative and positive ring potentials, were −0.7 V and 1.2 V in unbuffered electrolytes, respectively and −0.4 V and 1.2 V in pH 4 buffered electrolytes, respectively. The disc electrode potential scan rate was 5 mV s^{-1}. Arrows on ring currents represent potential scan direction.

pH 4 produces aqueous $V^{(IV)}$ species, which is also in agreement with the Pourbaix diagram (Fig. 2).

The results of RRDE experiments for NVPF show similar trends to NVP. In unbuffered electrolytes, the negatively polarized ring currents are about a factor of two lower than in NVP. This suggests that generally, NVPF is a more stable structure in aqueous media than NVP. The negative I_{ring} starts to significantly increase at the onset of an anodic disc wave but fades once the potential sweep direction is reversed. The observed positively polarized ring currents are similar, and about an order of magnitude lower than the negative ones. This indicates that in near neutral electrolytes $V^{(V)}$ is mostly generated during the electrochemical cycling of NVPF.

In pH 4 buffered electrolytes, the initial background current on the negatively polarized ring is almost ten times larger than in unbuffered 1 M Na_2SO_4 (aq.) (Figs. 7d vs 7c). The negative I_{ring} starts to increase well before the onset of anodic disc current peak which could be attributed to the reduction of chemically dissolved V species. On the positively polarized ring, the current values are about five times higher compared to those in a neutral electrolyte (Figs. 7d vs 7c). Interestingly, at pH 4, the positive I_{ring} peak positions are significantly shifted to negative direction with respect to NVPF disc current peaks (Fig. 7d). One of the possible explanations for this could be slightly stronger NVPF chemical dissolution during discharge rather than charge.

A set of identical RRDE experiments were also performed in a galvanostatic mode on NVP and NVPF disc electrodes. The specific currents of 0.59 A g^{-1} and 0.640 A g^{-1} corresponding to a rate of 5 C were used for NVP and NVPF, respectively. High charge/discharge rates were selected due to the time-limited nature of these experiments and found to be optimal in this particular case. The operating potential cut-offs of 0.3–0.8 V and 0.1–0.8 V vs Ag/AgCl were selected for NVP and NVPF, respectively. The data presented in Fig. 8 is in the form of dQ/dE vs E plot. The results indicate two reversible disc potential plateaus around 0.5 V and 0.7 V vs Ag/AgCl for NVP and NVPF, respectively. The potential plateaus in the NVP charge/discharge profiles are very flat, but slightly slanted in the case of NVPF. Overall, the galvanostatic RRDE results indicate very similar trends as the previously discussed experiments in the potentiodynamic mode. However, the noise observed in the ring currents is much higher. There is also an indication that ring current waves are much broader in the galvanostatic mode and even if they still correlate with the processes on the disc there seems to be some delay. Nevertheless, the recorded positive ring currents for NVP (Fig. 8b) and NVPF (Fig. 8d) jump by over an order of magnitude at pH 4 versus neutral system supporting our previous result that lower oxidation state vanadium species are generated in acidic electrolytes. The fact that negative currents are also high during discharging but not in all cases exceed those during charging still confirms that most likely $V^{(IV)}$ species are also present during degradation at low pH. These results might suggest that galvanostatic mode is not as suitable as potentiodynamic mode for this type of experiments. In a potentiodynamic mode, the main redox processes in the active material are accelerated during the potential scan resulting in substantially higher currents observed on the disc electrode. However, in a galvanostatic mode, the disc current is constant and the electrochemically induced degradation processes proceed more steadily over the potential range of operation. In turn, this results in more steady currents on the ring electrode which complicates the study of the degradation process in situ/operando.

The overall results obtained using RRDE technique explicitly suggest that in addition to chemical dissolution, there is a non-negligible electrochemically-induced generation of soluble $V^{(IV)}$ species at pH 4. The origin and stability of $V^{(IV)}$ species can be explained thermodynamically based on the Pourbaix diagram (Fig. 2) which suggests that $V^{(IV)}$ is favored over $V^{(V)}$ at lower pH values. Another possible explanation could be more mechanistic, and related to the co-insertion

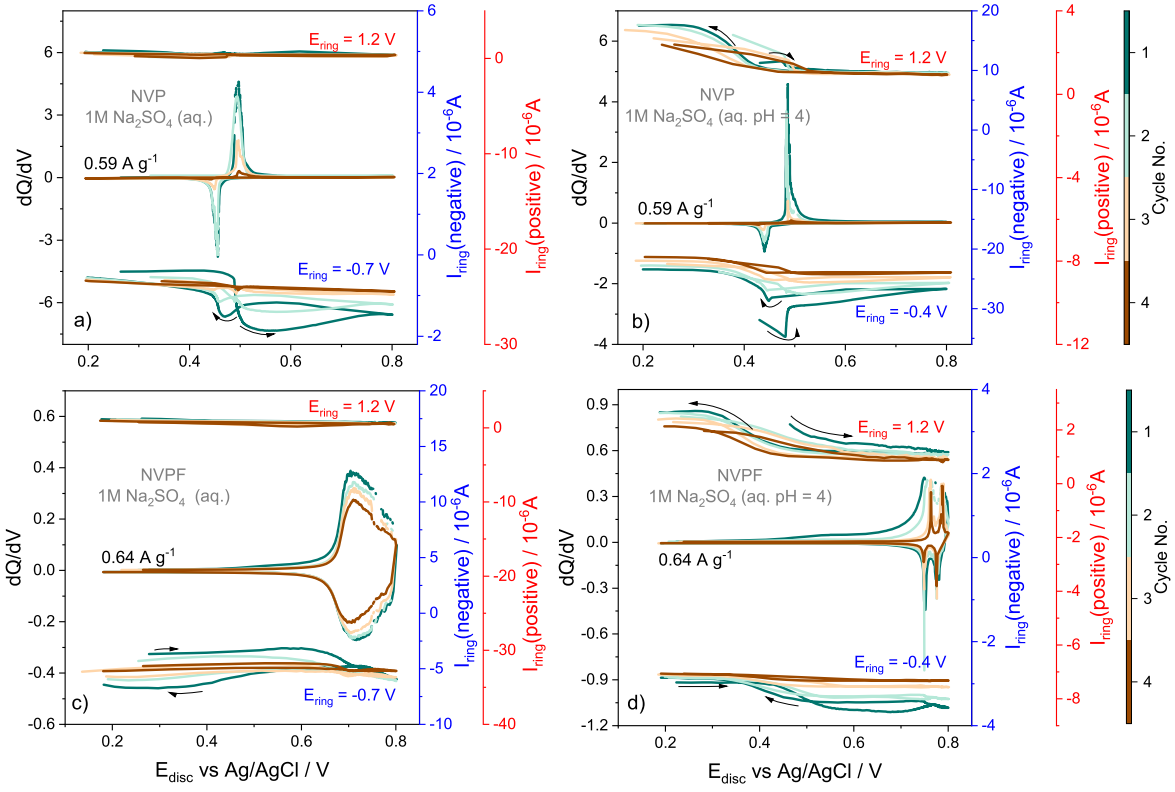

Figure 8. Galvanostatic cycling of RRDE disc electrode together with chronoamperograms of Pt ring electrode (right *y*-axes) corresponding to: (a) NVP in unbuffered 1 M Na_2SO_4 (aq.); (b) NVP in buffered 1 M Na_2SO_4 (aq. pH = 4), (c) NVPF in unbuffered 1 M Na_2SO_4 (aq.); (d) NVPF in buffered 1 M Na_2SO_4 (aq. pH = 4). Negative and positive ring potentials, were −0.7 V and 1.2 V in unbuffered electrolytes, respectively and −0.4 V and 1.2 V in pH 4 buffered electrolytes, respectively. The disc electrode potential scan rate was 5 mV s^{-1}. Arrows on ring currents represent potential scan direction.

of protons into the NASICON structure. The protons would tend to destabilize it and release reduced vanadium species into the electrolyte.[50]

Conclusions

In this work, aqueous degradation of vanadium-based $Na_3V_2(PO_4)_3$ and $Na_3V_2(PO_4)_2F_3$ phosphate framework materials are comprehensively studied and analyzed using a number of experimental techniques such as cyclic voltammetry, elemental analysis, post-mortem powder X-ray diffractometry, and rotating ring-disc electrode method. The cyclic voltammetry analysis of $Na_3V_2(PO_4)_3$ in conventional cell setup and post-mortem electrode characterization show that chemical vanadium dissolution due to electrodes being simply immersed in 1 M Na_2SO_4 (aq.) electrolyte is a significant contributor to the capacity and electrochemical activity degradation. On the contrary, the chemical dissolution of vanadium from $Na_3V_2(PO_4)_2F_3$ is found to be almost negligible. This suggests that anionic substitution by fluoride ions significantly increases the structural stability of phosphate framework materials in aqueous environments. The results obtained by the rotating ring-disc electrode technique in potentiodynamic and galvanostatic modes provide a valuable way to study $Na_3V_2(PO_4)_3$ and $Na_3V_2(PO_4)_2F_3$ degradation processes real time during electrochemical operation in situ/operando. The results unambiguously indicate that in near neutral electrolytes, both $Na_3V_2(PO_4)_3$ and $Na_3V_2(PO_4)_2F_3$ show a significant generation of soluble $V^{(V)}$ mostly during the charging process. However, lowering the electrolyte pH not only increases the chemical vanadium dissolution but also leads to the additional electrochemically-induced generation of soluble $V^{(IV)}$ species which further increases material degradation. The results indicate that $Na_3V_2(PO_4)_2F_3$ is a much more suitable positive electrode material than $Na_3V_2(PO_4)_3$ for aqueous systems. A carefully designed electrolyte with controlled proton and water activity either using highly concentrated or hybrid (with organic co-solvent) approach could enable the use of these materials in aqueous electrochemical devices.

Acknowledgments

This project has received funding from the European Regional Development Fund (Project No. 01.2.2-LMT-K-718-02-0005) under a grant agreement with the Research Council of Lithuania (LMTLT).

Author Contributions

The manuscript was written through contributions of all authors. All authors have given approval to the final version of the manuscript.

ORCID

Davit Tediashvili https://orcid.org/0000-0002-9674-991
Jurgis Pilipavičius https://orcid.org/0000-0002-0250-1488
Jurga Juodkazytė https://orcid.org/0000-0003-1265-8320
Linas Vilčiauskas https://orcid.org/0000-0002-1256-9777

References

1. B. Dunn, H. Kamath, and J.-M. Tarascon, "Electrical energy storage for the grid: a battery of choices." *Science*, **334**, 928 (2011).
2. Z. Zhu, T. Jiang, M. Ali, Y. Meng, Y. Jin, Y. Cui, and W. Chen, "Rechargeable Batteries for Grid Scale Energy Storage." *Chem. Rev.*, **122**, 16610 (2022).
3. M. Armand and J.-M. Tarascon, "Building better batteries." *Nature*, **451**, 652 (2008).
4. C. Bauer et al., "Charging sustainable batteries." *Nature Sustainability*, **5**, 176 (2022).
5. N. Tapia-Ruiz et al., "2021 Roadmap for sodium-ion batteries." *J. Phys. Energy*, **3**, 031503 (2021).
6. I. Hasa, S. Mariyappan, D. Saurel, P. Adelhelm, A. Y. Koposov, C. Masquelier, L. Croguennec, and M. Casas-Cabanas, "Challenges of today for Na-Based batteries of the future: from materials to cell metrics." *J. Power Sources*, **482**, 228872 (2021).
7. C. Delmas, "Sodium and sodium-ion batteries: 50 years of research." *Adv. Energy Mater.*, **8**, 1703137 (2018).
8. C. Masquelier and L. Croguennec, "Polyanionic (phosphates, silicates, sulfates) frameworks as electrode materials for rechargeable Li (or Na) batteries." *Chem. Rev.*, **113**, 6552 (2013).
9. T. Jin, H. Li, K. Zhu, P.-F. Wang, P. Liu, and L. Jiao, "Polyanion-type cathode materials for sodium-ion batteries." *Chem. Soc. Rev.*, **49**, 2342 (2020).
10. S. Chen, C. Wu, L. Shen, C. Zhu, Y. Huang, K. Xi, J. Maier, and Y. Yu, "Challenges and perspectives for NASICON-type electrode materials for advanced sodium-ion batteries." *Advanced Materials*, **29**, 1700431 (2017).
11. C. Delmas, R. Olazcuaga, F. Cherkaoui, R. Brochu, and G. Le Flem, "Cheminform Abstract: A New Family of Phosphates with the Formula $Na_3M_2(PO_4)_3$ (M = Ti, V, Cr, Fe)." *Chem. Inf.*, **10**, N/A (1979).
12. Z. Jian et al., "Superior electrochemical performance and storage mechanism of Na3V2(PO4)3Cathode for room-temperature sodium-ion batteries." *Adv. Energy Mater.*, **3**, 156 (2013).
13. C. Zhu, K. Song, P. A. van Aken, J. Maier, and Y. Yu, "Carbon-coated Na3V2 (PO4)3 embedded in porous carbon matrix: an ultrafast na-storage cathode with the potential of outperforming Li Cathodes." *Nano Lett.*, **14**, 2175 (2014).
14. J. P. Allen and C. P. Grey, "Solution NMR of battery electrolytes: assessing and mitigating spectral broadening caused by transition metal dissolution." *J. Phys. Chem. C Nanomater. Interfaces*, **127**, 4425 (2023).
15. T. Broux, T. Bamine, L. Simonelli, L. Stievano, F. Fauth, M. Ménétrier, D. Carlier, C. Masquelier, and L. V. I. V. Croguennec, "Disproportionation upon sodium extraction from Na3V2(PO4)2F3 observed by operando X-ray absorption spectroscopy and solid-state NMR." *J. Phys. Chem. C*, **121**, 4103 (2017).
16. E. Boivin, J.-N. Chotard, C. Masquelier, and L. Croguennec, "Towards reversible high-voltage multi-electron reactions in alkali-ion batteries using vanadium phosphate positive electrode materials." *Molecules*, **26**, 1428 (2021).
17. T. Broux et al., "High Rate Performance for Carbon-Coated $Na_3V_2(PO_4)_2F_3$ in Na-ion batteries." *Small Methods*, **3**, 1800215 (2019).
18. P. Desai, J. Forero-Saboya, V. Meunier, G. Rousse, M. Deschamps, A. M. Abakumov, J.-M. Tarascon, and S. Mariyappan, "Mastering the synergy between $Na_3V_2(PO_4)_2F_3$ electrode and electrolyte: a must for Na-Ion cells." *Energy Storage Materials*, **57**, 102 (2023).
19. W. Song, X. Ji, Y. Zhu, H. Zhu, F. Li, J. Chen, F. Lu, Y. Yao, and C. E. Banks, "Aqueous Sodium-Ion battery using a $Na_3V_2(PO_4)_3$ Electrode." *ChemElectroChem*, **1**, 871 (2014).
20. R. Demir-Cakan, M. Rosa Palacin, and L. Croguennec, "Rechargeable aqueous electrolyte batteries: from univalent to multivalent cation chemistry." *J. Mater. Chem. A Mater. Energy Sustain.*, **7**, 20519 (2019).
21. L. Sharma and A. Manthiram, "Polyanionic insertion hosts for aqueous rechargeable batteries." *J. Mater. Chem. A Mater. Energy Sustain.*, **10**, 6376 (2022).
22. J. Cao, Y. Wang, L. Wang, F. Yu, and J. Ma, "$Na_3V_2(PO_4)_3$@C as faradaic electrodes in capacitive deionization for high-performance desalination." *Nano Lett.*, **19**, 823 (2019).
23. C. Zhan, T. Wu, J. Lu, and K. Amine, "Dissolution, migration, and deposition of transition metal ions in Li-Ion batteries exemplified by Mn-based cathodes—a critical review." *Energy Environ. Sci.*, **11**, 243 (2018).
24. Y. Sui and X. Ji, "Anticatalytic strategies to suppress water electrolysis in aqueous batteries." *Chem. Rev.*, **121**, 6654 (2021).
25. Z. Liu, Y. Huang, Y. Huang, Q. Yang, X. Li, Z. Huang, and C. Zhi, "Voltage issue of aqueous rechargeable metal-ion batteries." *Chem. Soc. Rev.*, **49**, 180 (2020).
26. D. Wu et al., "2022 Roadmap on aqueous batteries." *J. Phys. Energy*, **4**, 041501 (2022).
27. H. Zhang, X. Tan, H. Li, S. Passerini, and W. Huang, "Assessment and progress of polyanionic cathodes in aqueous sodium batteries." *Energy Environ. Sci.*, **14**, 5788 (2021).
28. W. Yang, B. Wang, Q. Chen, Q. Zhao, Q. Zhang, S. Lu, Y. Gao, X. Wang, Q. Xie, and Y. Ruan, "Unravelling capacity fading mechanisms in sodium vanadyl phosphate for aqueous sodium-ion batteries." *J. Colloid Interface Sci.*, **627**, 913 (2022).
29. C. Zech, M. Evertz, M. Börner, Y. Kayser, P. Hönicke, M. Winter, S. Nowak, and B. Beckhoff, "Quantitative manganese dissolution investigation in lithium-ion batteries by means of X-ray spectrometry techniques." *J. Anal. At. Spectrom.*, **36**, 2056 (2021).
30. L. Hanf, J. Henschel, M. Diehl, M. Winter, and S. Nowak, "Mn^{2+} or Mn^{3+}? Investigating transition metal dissolution of manganese species in lithium ion battery electrolytes by capillary electrophoresis." *Electrophoresis*, **41**, 697 (2020).
31. J. P. Allen and C. P. Grey, "Determining the oxidation states of dissolved transition metals in battery electrolytes from solution NMR spectra." *Chem. Commun.*, **59**, 1677 (2023).
32. S. J. Wachs, C. Behling, J. Ranninger, J. Möller, K. J. J. Mayrhofer, and B. B. Berkes, "Online monitoring of transition-metal dissolution from a High-Ni-Content cathode material." *ACS Appl. Mater. Interfaces*, **13**, 33075 (2021).
33. J. Ranninger, S. J. Wachs, J. Möller, K. J. J. Mayrhofer, and B. B. Berkes, "On-line monitoring of dissolution processes in nonaqueous electrolytes—a case study with platinum." *Electrochem. commun.*, **114**, 106702 (2020).
34. D. C. Bock, A. C. Marschilok, K. J. Takeuchi, and E. S. Takeuchi, "A kinetics and equilibrium study of vanadium dissolution from vanadium oxides and phosphates in battery electrolytes: possible impacts on ICD battery performance." *J. Power Sources*, **231**, 219 (2013).
35. T.-N. Kröger, S. Wiemers-Meyer, P. Harte, M. Winter, and S. Nowak, "Direct multielement analysis of polydisperse microparticles by classification-single-particle ICP-OES in the field of lithium-ion battery electrode materials." *Anal. Chem.*, **93**, 7532 (2021).
36. T. Paljk, V. Bracamonte, T. Syrový, S. D. Talian, S. Hočevar, and R. Dominko, "Integrated sensor printed on the separator enabling the detection of dissolved manganese ions in battery cell." *Energy Storage Materials*, **55**, 55 (2023).
37. D. Tediashvili, G. Gečė, J. Pilipavičius, S. Daugėla, T. Šalkus, J. Juodkazytė, and L. Vilčiauskas, "Synthesis, characterization, and degradation study of Mn-based

phosphate frameworks ($Na_3MnTi(PO_4)_3$, $Na_3MnPO_4CO_3$, $Na_4Mn_3(PO_4)_2P_2O_7$) as Aqueous Na-Ion battery positive electrodes." *Electrochim. Acta*, **417**, 140294 (2022).
38. C. J. Clarke, G. J. Browning, and S. W. Donne, "An RDE and RRDE study into the electrodeposition of manganese dioxide." *Electrochim. Acta*, **51**, 5773 (2006).
39. T. N. T. Tran, S. Jin, M. Cuisinier, B. D. Adams, and D. G. Ivey, "Reaction mechanisms for electrolytic manganese dioxide in rechargeable aqueous zinc-ion batteries." *Sci. Rep.*, **11**, 20777 (2021).
40. L.-F. Wang, C.-C. Ou, K. A. Striebel, and J.-S. Chen, "Study of Mn dissolution from $LiMn_2O_4$ spinel electrodes using rotating ring-disk collection experiments." *J. Electrochem. Soc.*, **150**, A905 (2003).
41. N. Todoroki, H. Tsurumaki, H. Tei, T. Mochizuki, and T. Wadayama, "Online electrochemical mass spectrometry combined with the rotating disk electrode method for direct observations of potential-dependent molecular behaviors in the electrode surface vicinity." *J. Electrochem. Soc.*, **167**, 106503 (2020).
42. P. Serras, V. Palomares, J. Alonso, N. Sharma, J. M. López del Amo, P. Kubiak, M. L. Fdez-Gubieda, and T. Rojo, "Electrochemical Na extraction/insertion of $Na_3V_2O_{2x}(PO_4)_2F_{3-2x}$." *Chem. Mater.*, **25**, 4917 (2013).
43. Y.-U. Park, D.-H. Seo, B. Kim, K.-P. Hong, H. Kim, S. Lee, R. A. Shakoor, K. Miyasaka, J.-M. Tarascon, and K. Kang, "Tailoring a fluorophosphate as a novel 4 V cathode for lithium-ion batteries." *Sci. Rep.*, **2**, 704 (2012).
44. B. K. Hodnett, P. Permanne, and B. Delmon, "Influence of P/V ratio on the phase composition and catalytic activity of vanadium phosphate based catalysts." *Appl. Catal.*, **6**, 231 (1983).
45. B. Zhang, R. Dugas, G. Rousse, P. Rozier, A. M. Abakumov, and J.-M. Tarascon, "Insertion compounds and composites made by ball milling for advanced sodium-ion batteries." *Nat. Commun.*, **7**, 10308 (2016).
46. X. Yao, Z. Zhu, Q. Li, X. Wang, X. Xu, J. Meng, W. Ren, X. Zhang, Y. Huang, and L. Mai, "3.0 V high energy density symmetric sodium-ion battery: $Na_4V_2(PO_4)_3\|Na_3V_2(PO_4)$." *ACS Appl. Mater. Interfaces*, **10**, 10022 (2018).
47. I. Povar, O. Spinu, I. Zinicovscaia, B. Pintilie, and S. Ubaldini, "Revised Pourbaix diagrams for the vanadium—water system." *J. Electrochem. Sci. Eng.*, **9**, 75 (2019).
48. G. Plečkaitytė, M. Petrulevičienė, L. Staišiūnas, D. Tediashvili, J. Pilipavičius, J. Juodkazytė, and L. Vilčiauskas, "Understanding and mitigation of $NaTi_2(PO_4)_3$ degradation in aqueous Na-ion batteries." *J. Mater. Chem. A Mater. Energy Sustain.*, **9**, 12670 (2021).
49. T. Jenkins, J. A. Alarco, B. Cowie, and I. D. R. Mackinnon, "Direct spectroscopic observation of the reversible redox mechanism in $A_3V_2(PO_4)_3$(A=Li,Na) cathode materials for Li-Ion batteries." *J. Power Sources*, **571**, 233078 (2023).
50. W. Li, X. Jing, K. Jiang, and D. Wang, "Observation of structural decomposition of $Na_3V_2(PO_4)_3$ and $Na_3V_2(PO_4)_2F_3$ as cathodes for aqueous Zn-ion batteries." *ACS Appl. Energy Mater.*, **4**, 2797 (2021).